Effect of depositional water content on the collapsibility of a reconstituted loess

Ling Xin Wong[1], Tom Shire[2,*] and Jamie Standing[3]

Abstract

Loess, a wind-blown silty soil, can be deposited under a variety of moisture conditions, including dry deposition, wet deposition and gravitational settling of aggregations formed in moist air by capillary forces at grain contacts. This experimental study uses single and double oedometer tests to assess the effect of depositional water content on the collapse potential of reconstituted samples of the Langley Silt Member, known as Brickearth, a natural loessic soil. A freefall sample preparation technique was used to mimic loess formation and environmental scanning electron microscopy was used to relate the observed behaviour to sample fabric. The results show that loess deposited at higher water contents has a greater collapse potential, which is shown to be related to its looser, more granular fabric.

1: Buro Happold, London, UK

2: University of Glasgow, UK

3: Imperial College London, UK

*: thomas.shire@glasgow.ac.uk

Introduction

Loess is an aeolian (wind-blown) deposit that comprises predominantly silt-sized particles and is widely distributed in arid and semi-arid regions; it covers about 10% of the Earth's land surface. Loessic soils typically have an open honeycomb structure with a high void ratio (Sides and Barden, 1971). In their natural state, these soils are unsaturated and show high apparent strength, i.e. they are stable at their in-situ water contents. However, they can be susceptible to hydro-collapse or wetting-induced collapse, a process where they undergo a rapid reduction in volume when they are loaded and wetted (Feda, 1988; Northmore et al., 1996; Milodowski et al., 2015).

Loess and other collapsible soils typically consist of predominantly silt size particles which might be bound together by clay bridges through capillary suction, or cementation by subsequent deposition of calcium carbonate (Barden et al., 1973; Li et al., 2016). Although loessic soils are transported by the wind, they can be deposited under a range of moisture conditions, including *(i)* dry deposition due to a reduction in wind speed or increase in surface roughness; *(ii)* wet deposition due to precipitation; *(iii)* formation and gravitational settling of grain aggregations formed when atmospheric moisture causes agglomeration of individual particles (Pye, 1995; Iriondo and Kröhling, 2007); *(iv)* reworked and redeposited by fluvial processes (Northmore et al., 1996). The fabric of the initially deposited loess will have a major influence on the post-depositional processes of loessification, such as the accumulation of illuviated clay and/or calcite crystal formation at clay bridges between particles formed during deposition (Smalley and Marković, 2014; Milodowski et al., 2015).

While previous work on the collapsibility of loess has sought to reproduce the conditions under which loess forms (Zourmpakis et al., 2005; Jefferson and Ahmad, 2007) or the fabric of in-situ loess (Jiang et al. 2012), the effect of depositional water content on the engineering behaviour of loess has not been studied. This research, therefore, aims to explore the behaviour of a reconstituted loessic soil formed from the Langley Silt Member, previously known as Brickearth, under a variety of depositional water contents. Single and double oedometer tests (Jennings and Knight, 1975) were used to determine the collapsibility and environmental scanning electron microscopy (ESEM) was used to analyse qualitatively the soil fabric at the micro-scale before and after collapse.

Materials and Methods

Langley Silt Member

Langley Silt Member (BGS, 2016), commonly known as Brickearth, is a yellow-brown slightly clayey silt which is present in central London and west to Slough and south to Battersea. It is generally deposited above the Kempton Park and Taplow Gravel members. Although originally a loess deposit, the soil was subsequently reworked and redeposited under alluvial conditions, thus destroying its early structure (Rose et al. 2000, Milodowski et al. 2015, BGS 2016). Block samples of the soil tested here

were excavated from beneath St Paul's Cathedral during the construction of a shaft to provide lift access to the crypt. Standard classification tests were carried out in accordance with BS1377 (British Standards Institution, 1990). The particle size distribution is given in Figure 1 and consists of 19% clay, 70% silt and 11% fine sand. The liquid limit is w_L = 31% and plasticity index is I_P = 13%, giving a classification of low plasticity clay.

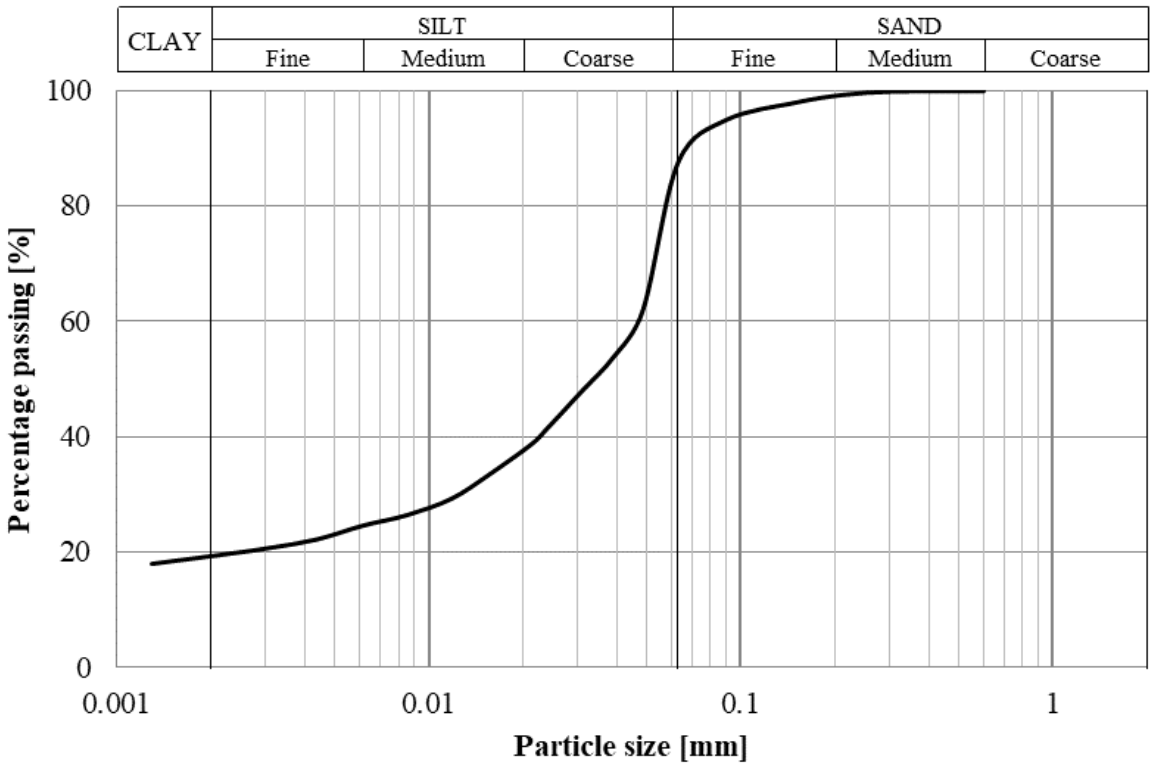

Figure 1. Particle size distribution

Preparation of artificial loess

Previous methods of preparing artificial loess samples have been summarised by Jefferson and Ahmad (2007). The new method used here utilises ideas from the dry sieving method (Assallay, 1998) and the wet method (Jefferson and Ahmad, 2007).

Soil samples were dried and ground to a powder using a pestle and mortar. Checks were conducted to ensure that there was no change in particle size distribution. They were then mixed to a range of nominal water contents (w_n) using high purity water produced by a Purite RO50 reverse osmosis system. A very fine mister was used to ensure an even distribution of water and the soil was mixed thoroughly using an electric mixer with twin beaters. The mixed soil was sealed in plastic bags for at least 24 h to allow water content equilibration. The mixed water content w_i was determined for a sub-sample of each mixture and values are presented in Table 1. The sample with a nominal water content w_n = 0% had an initial water content around w_i = 1.5%, which is the equilibrium water content at a laboratory relative

humidity of RH ≈ 70% and temperature of 20 °C. The other samples were typically within ±0.5% of the nominal water content. As the mixture water content increased, the samples formed larger aggregations, from a predominantly silt-sized fine powder at w_n = 0% to aggregations of coarse sand to fine gravel size at w_n = 18%.

Artificial loess samples were prepared as follows.

1. Prepared soil is deposited into a 50 mm diameter steel oedometer ring by freefall through a 0.63 mm aperture sieve from a height of 200 mm.
2. Once the ring is half full, the soil is statically compacted in the oedometer cell to σ_v = 32 kPa for 15 minutes to simulate an arbitrary overburden of 2 m.
3. More soil is deposited through the sieve until the ring is then filled. The surface is levelled off and the sample is compacted as before.
4. A third layer of soil is sieved into the ring until full, and it is levelled off and compacted again.
5. The sample is left to air dry with its mass recorded on a data-logged weighing scale until it stabilises. This indicates that the sample has reached its residual water content, which in each case was $w_{res} \approx$ 1.5%. The Langley Silt Member samples undergo very little shrinkage and negligible cracking during drying. The lack of shrinkage during drying was one of the properties that made loessic deposits such as the Langley Silt Member well suited to brick production.

Oedometer testing

Double and single oedometer tests (Jennings and Knight, 1975) were carried out using a standard front-loaded oedometer, closely following standard procedures (Jennings and Knight, 1975; Head and Epps, 2011). In the double oedometer tests, dry samples (series F_{1600}) were loaded in stages to σ_v = 1600 kPa at the residual water content and then flooded with water. The results from the series F_{1600} tests are compared with those from series F_{12} tests where samples were flooded shortly after applying a load of σ_v = 12 kPa before being loaded in stages to σ_v = 1600 kPa. In the single oedometer tests (series F_{200}), dry samples were loaded in stages to σ_v = 100 kPa before being flooded shortly after applying a load of σ_v = 200 kPa and then subsequently loaded in stages to σ_v = 1600 kPa.

The flooding of samples shortly after loading in the F_{12}- and F_{200}-series tests is a deviation from normal practice (e.g. Jennings and Knight, 1975), in which flooding is carried out after a full unsaturated loading stage. However, the agreement between the single and double oedometer test results and the repeatability of the data suggest that collapse settlement values equivalent to those obtained using normal practice can be obtained from the data. All samples were unloaded in stages to σ_v = 12 kPa. In the case of the F_{12}- and F_{200}-series tests at w_n = 12%, there was an experimental mishap during the unloading stage and so the data from these tests are not reported.

To investigate the micro-scale fabric further, specimens were prepared from oedometer samples for the F_{1600}-series tests with w_n = 0% and 12% for imaging with a FEI Quanta 200F Environmental Scanning

Electron Microscope (ESEM) for two test stages: *(i)* following compression to σ_v = 1600 kPa but before flooding and *(ii)* after flooding following compression to σ_v = 1600 kPa.

Results

Sample water content

The water content of prepared soil which had fallen just outside the oedometer ring, w_{prep}, is compared with the mixed water content (prior to deposition), w_i, in Table 1. With the exception of the sample at residual water content, the prepared water contents are lower than the mixture water contents, and the higher the mixture water content the higher the reduction in water content during preparation ($w_i - w_{prep}$). This reduction is partly due to evaporation, and partly due to the larger, wetter aggregations being too large to pass through the 0.63 mm sieve during preparation. Figure 2 shows the roughly linear relationship between prepared water content, w_{prep}, and the initial void ratio just prior to oedometer testing. A limiting value of just below w_{prep} = 9% was found using this technique. Note that there are three points for each w_n value as three samples were prepared for the three oedometer tests performed for each w_n value, as discussed in the next section. The w_{prep} values given in Table 1 are the averages from the sets of three.

Nominal water content, w_n (%)	Mean mixture water content, w_i (%)	Mean prepared water content (after free-fall), w_{prep} (%)	Initial void ratio following final compaction at σ_v = 32 kPa, e_0	Void ratio at σ_v = 1600 kPa, flooded, e_{1600}	Collapse index, I_e (%)
0	1.5	1.5	1.029	0.415	12.7
3	3.3	3.1	1.060	0.400	19.1
6	5.8	5.0	1.326	0.431	24.6
9	8.5	7.3	1.547	0.387	32.9
12	11.6	7.5	1.628	0.381	-
15	14.1	8.4	1.796	0.365	40.5
18	17.8	8.0	1.736	0.398	35.3

Table 1. Properties of artificial loess samples. Note void ratio values are taken from the F_{200} test series

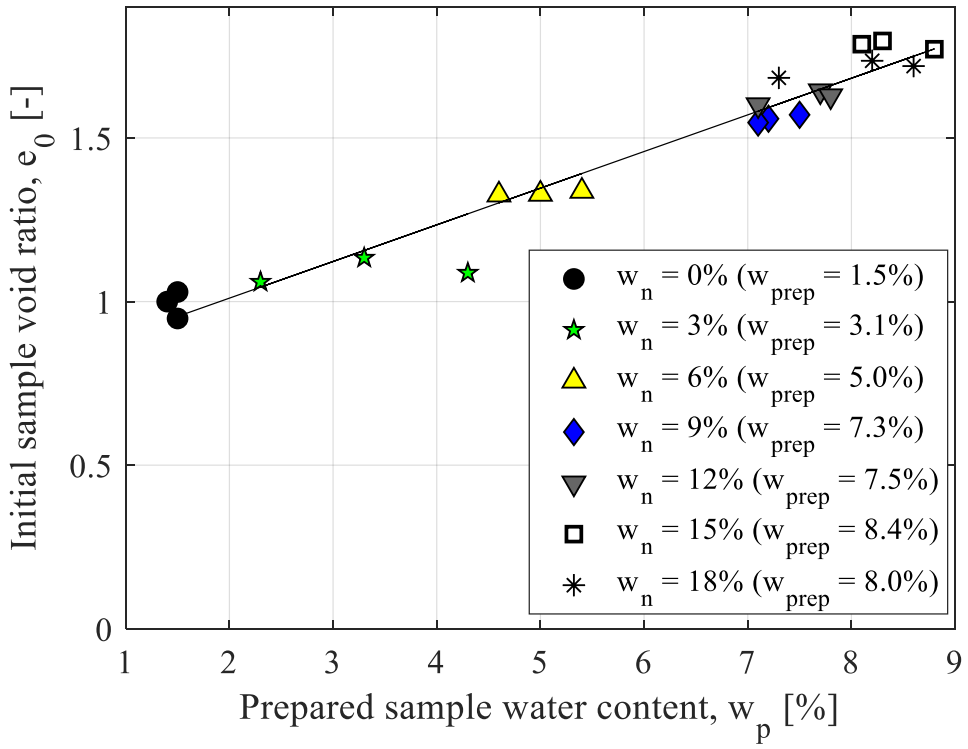

Figure 2. Relationship between prepared water content (after free-fall) and initial void ratio

One dimensional compression testing

Figure 3 shows the compression curves (void ratio vs vertical stress) for w_n = 6%. The F_{200}-series test follows the F_{1600}-series curve until flooding, after which it follows the F_{12}-series curve. This trend was found at all water contents, confirming the repeatability of the testing procedure. The F_{1600}- and F_{200}-series tests are seen to yield at around σ_v = 50 kPa, whereas the F_{12}-series test does not yield pre-wetting and follows an approximately linear normal compression line (NCL) to 1600 kPa. As a consequence of the near-simultaneous loading and wetting of the F_{12}- and F_{200}-series tests, it is not possible to distinguish between the effects of loading and flooding on sample compression. Therefore, the compression curves during the flooding stage in Figures 3 to 5 reflect the compression from both the new loading and the wetting together. The component of compression from the new loading alone can be reliably estimated from the amount of compression that occurred for the same load increment in the F_{1600}-series test as shown by the red dashed lines. This can be justified by the quality and repeatability of the data from the test series performed at the numerous water content values, where for a given nominal water content in all cases the F_{200}-series data are consistent with the F_{1600}-series data up to the point of wetting; and with the F_{12}-series data after the point of wetting. In order to show the effect of the wetting-induced collapse alone, blue broken lines have been constructed extending a distance vertically to reflect the total compression less the load compression component established during the F_{1600}-series tests.

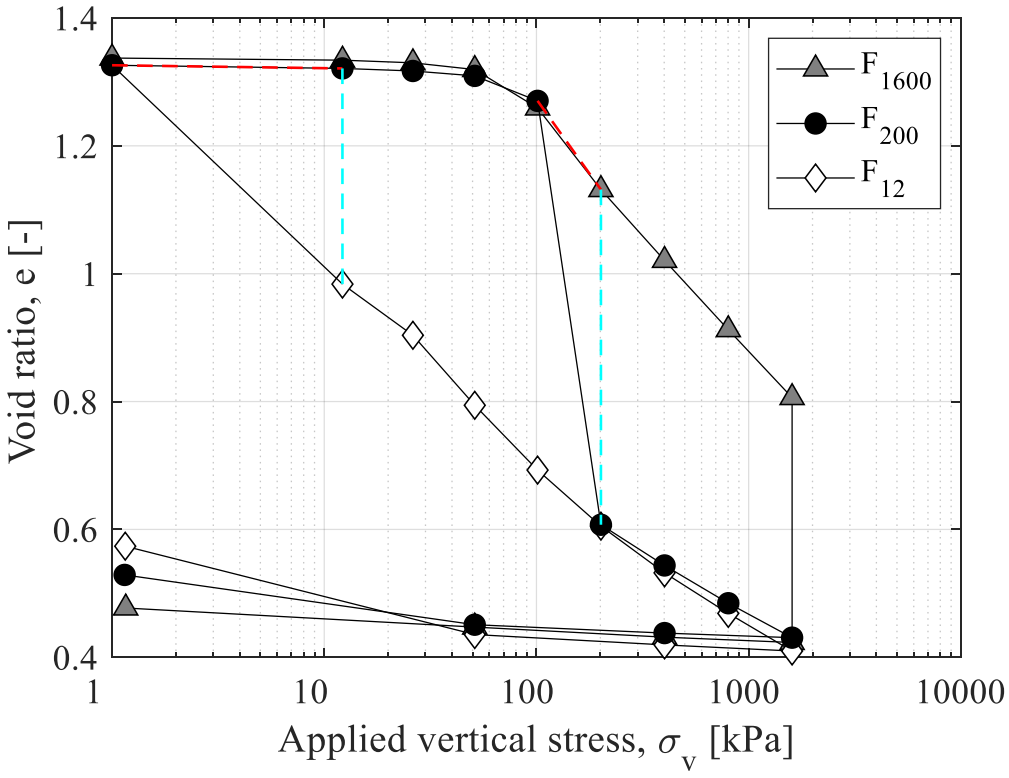

Figure 3. Compression curve for single and double oedometer test with nominal water content w_n = 6%. Red lines show the inferred compression due to loading and blue lines show the inferred compression due to flooding during the combined loading/flooding stage.

Figure 4 shows all the compression curves at each water content for each test series, and these are normalised by e_0 in Figure 5. The initial sample void ratio, e_0 increases with initial soil water content until w_n ≈15% and then decreases slightly for w_n ≈18%, mirroring the relationship between w_{prep} and e_0 shown in Figure 2. It should be noted that values of the initial void ratio in Figures 3 to 5 are shown at a nominal negligible applied vertical stress of 1 kPa while in reality they were measured under zero load. It can be seen, e.g. from Figures 5a and 5c, that the lines connecting the points at 1 kPa and 12 kPa are essentially horizontal for all w_n values, justifying this method of presentation.

For each test series, flooded samples reached a post-collapse void ratio at σ_v = 1600 kPa of $e_{1600} \approx 0.4$. In the F_{12}-series tests (flooded at σ_v =12 kPa), samples with higher e_0 had higher post-collapse void ratios (Figure 4b) and were initially more compressible following wetting, indicating that they do not fully collapse at σ_v =12 kPa. The F_{200}-series tests (flooded at σ_v =200 kPa) all collapsed to e ≈ 0.6 after wetting, approximately the same void ratio as the F_{12}-series samples at σ_v = 200 kPa. Tests from each series have similar swelling behaviour, with F_{12}-series samples tending to swell slightly more at low stresses.

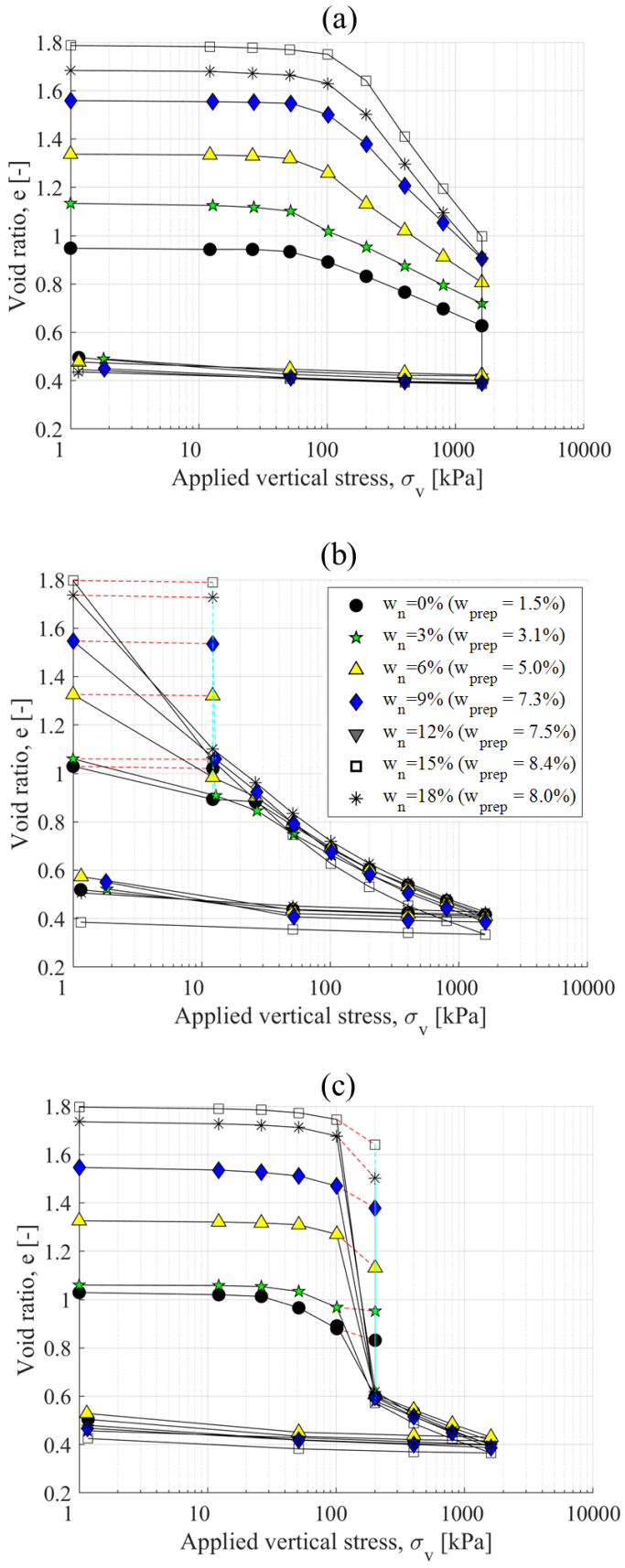

Figure 4. Compression curves at all nominal water contents. (a) F_{1600}-series; (b) F_{12}-series; (c) F_{200}-series. Red lines show the inferred compression due to loading and blue lines show the inferred compression due to flooding during combined loading/flooding stages.

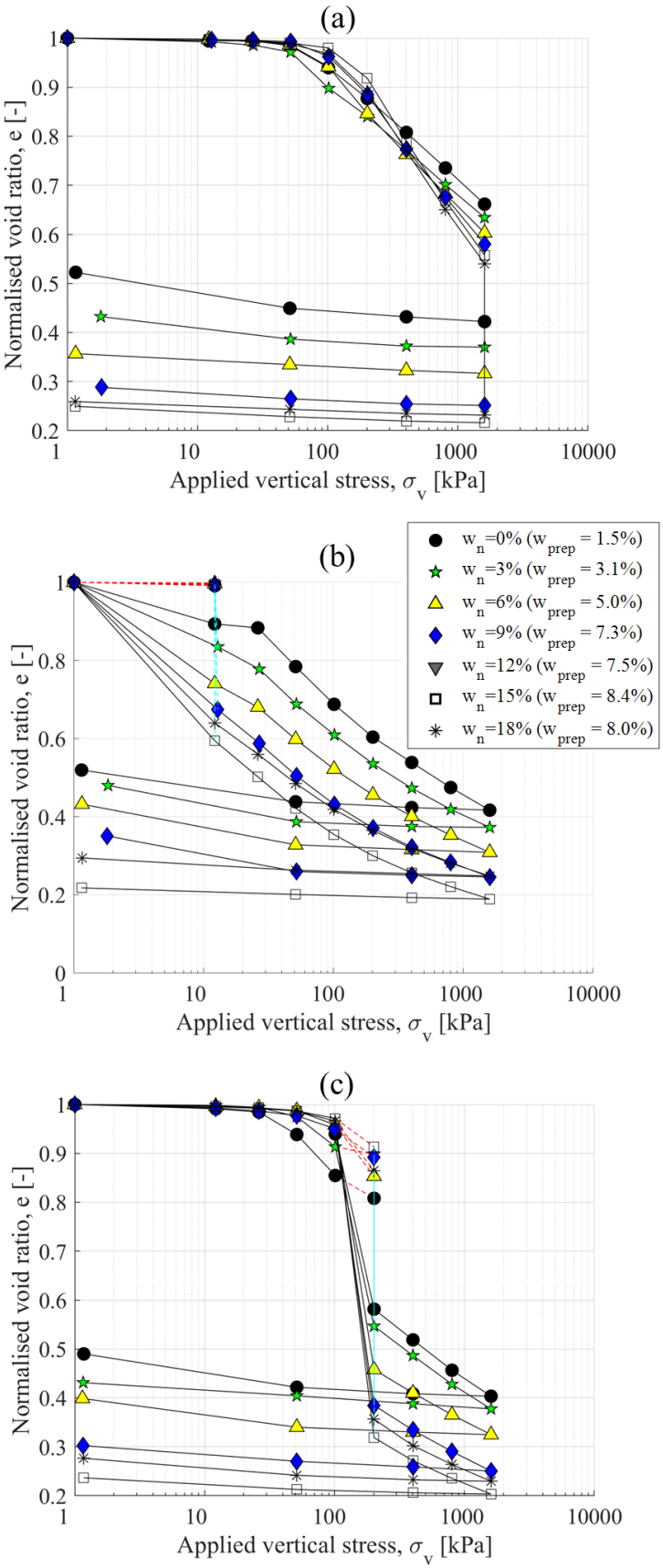

Figure 5. Normalised compression curves at all nominal water contents (a) F_{1600}-series; (b) F_{12}-series; (c) F_{200}-series. Red lines show the inferred compression due to loading and blue lines show the inferred compression due to flooding during combined loading/flooding stages.

Collapse potential

Collapse Potential (CP) is defined as:

$$CP = \frac{\Delta e}{1 + e_1} \tag{2}$$

where Δe is the change in void ratio following flooding and e_1 is the void ratio pre-flooding. Collapse Potential at σ_v = 200 kPa is defined as the Collapse Index I_e (ASTM International, 2014). For the F_{12}- and F_{200}-series, samples were flooded shortly after loading and so for these samples e_1 was estimated based on F_{1600}-series results (as described above). Note that a separation of loading and flooding stages in line with standard practice (Jennings and Knight, 1975) would allow the actual collapse potential to be calculated with full confidence. Estimated collapse potential is plotted against prepared water contents in Figure 6 and values of estimated I_e are given in Table 1. Estimated collapse potential is highest when samples are flooded at σ_v = 200 kPa, at which point there is sufficient load to cause significant collapse, but samples have not significantly yielded. This is more pronounced with higher values of w_{prep}, possibly because the reduction in void ratio between σ_v = 200 kPa and σ_v = 1600 kPa, due to loading in the dry state, is greater in these samples (see Figures 4a and 5a). In Figure 6 it can be seen that there is an approximately linear relationship between w_{prep} and estimated collapse potential up to the limiting value of $w_{prep} \approx 9\%$. All samples are classified by ASTM D5333-03 (ASTM International, 2003) as having the potential for severe collapse, which is unsurprising given the low compaction pressure applied and the loessic origin of the soil. This is higher than recorded values for the block samples of the Langley Silt Member and of other natural loess soils in south-east England and northern France (Muñoz-Castelblanco et al. 2011, Milodowski et al. 2015), whose geological history is likely to have led to partial collapse.

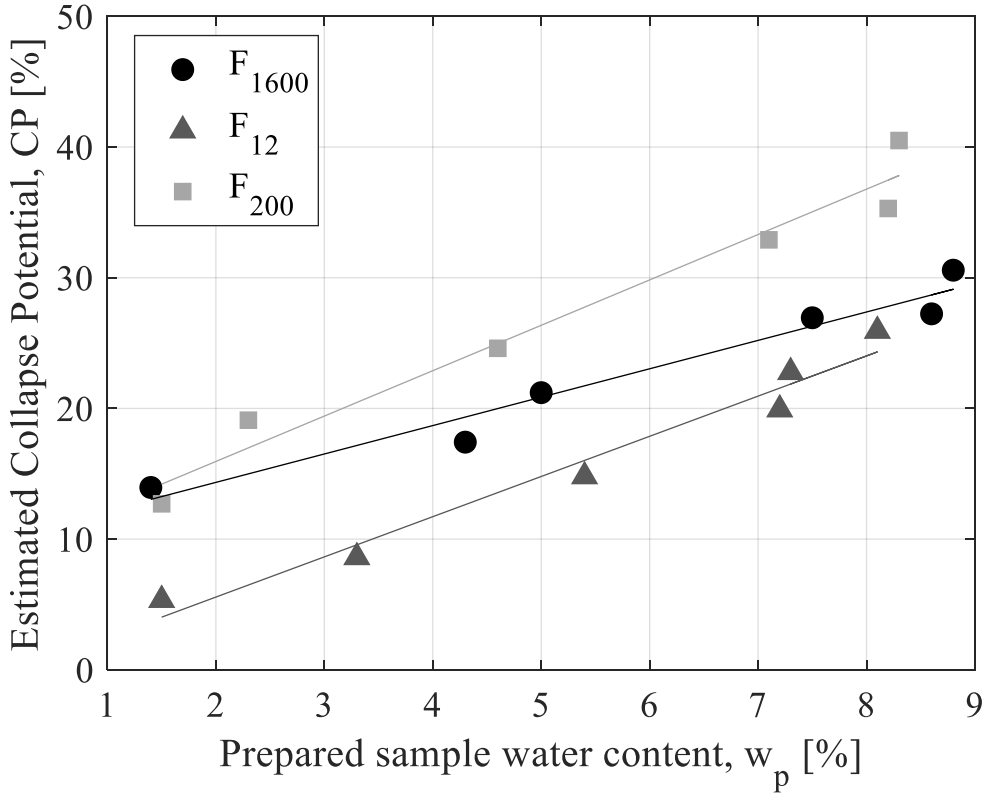

Figure 6. Variation of estimated collapse potential with prepared water content

Discussion

Key observations from the oedometer tests are that as prepared water content w_{prep} increases, the initial void ratio e_0 and hence estimated collapse potential increase. Figure 7 shows photographs of the fabric in the oedometer ring post-freefall. Wetter samples have larger individual aggregations and are also darker (note that this darker colour was retained even after oven drying (Wong, 2017). ESEM images of samples for the F_{1600}-series tests prepared with w_n = 0% and 12% are presented in Figure 8. The pre-flooding fabric of the less collapsible sample (w_n = 0%) is shown in Figure 8(a). Clay particles connect angular silt grains into larger aggregations. Many silt grains are connected by point to point contacts, suggesting that there are only a few bonds at interparticle contacts (Li et al., 2016). There are many small pores within the clay aggregations, but fewer large macro-pores, which helps to explain to some extent the lower void ratio of the w_n = 0% sample compared with samples deposited at higher water contents. It can be inferred that due to the lower depositional water content there is insufficient moisture to produce extensive clay bridges at contact points and, therefore, interparticle contacts play a key role in transferring load.

In contrast, the more collapsible sample (w_n = 12%) shown in Figure 8(c) is formed of aggregations of up to approximately 100 μm. These are formed of silt particles 'clothed' with clay (Barden et al., 1973), which appear more rounded than the exposed silt grains in Figure 8(a). In Figure 8(c) there are large

voids between the coated silt grains, whose structure is sustained primarily by meniscus forces at the contacts. The overall matrix is more porous (i.e. has a higher void ratio) with fewer clayey aggregations than the sample prepared at the lower water content. This open fabric of clay-coated silt particles is similar to that observed in undisturbed loessic deposits from Ospringe by Milodowski et al. (2015), as shown in Figure 8(e). However, other structures of a post-depositional nature, such as meniscus bridges reinforced by illuviated clay and calcite scaffolding, could not be created using the methodology used here.

The post-flooding fabrics of the two samples were indistinguishable in the ESEM (see Figure 8(b) and (d)), due to the high level of reworking due to shearing associated with collapse at σ_v = 1600 kPa. In both samples the clay matrix is dominant and there is a much less open structure with relatively few macro-pores. The silt grains appear aligned and provide a close-packed structure which will limit further rearrangement.

Limited collapse tests were carried out on intact samples of the same Langley Silt as part of another project. The intact void ratios of these samples were in the range of 0.66 to 0.69 and the post-collapse void ratio values at σ_v = 1600 kPa were around 0.4, similar to those reported in this study. This is consistent with the origin of Langley Silt Member material which has been reworked and redeposited by alluvial processes from a loessic source material (Rose et al. 2000, BGS 2016).

Conclusions

A series of laboratory experiments has been carried out in order to investigate the effect of depositional water content on the collapse behaviour of loess. The material tested was taken from disturbed samples of loessic deposits, and was prepared for testing using an aerial freefall technique. This can create clay bridge fabrics which are similar to those found in natural loess (Milodowski et al., 2015; Li et al., 2016) and was shown to produce repeatable results, which is important for developing constitutive models of soil behaviour. However, one-dimensional compression testing should ensure that separate loading and flooding stages are used in line with standard practice (Jennings and Knight, 1975).

From the oedometer and ESEM results presented, the following observations about the effect of depositional water content on loessic soils can be made.

- The samples deposited at higher water contents tend to have a structure consisting of aggregations of clay-clothed silt of dimension up to 100 μm, whereas when deposited at lower water contents they have a structure more strongly dominated by larger aggregations of silt grains connected by clay particles and by interparticle contacts between silt particles.
- When flooded at low vertical stresses (σ_v = 12 kPa), samples deposited at higher water contents will collapse to higher void ratios than samples prepared at lower water contents and be more compressible when loaded further.

- When flooding-induced collapse occurs at vertical stresses higher than the yield stress, samples deposited at different water contents will collapse to the same void ratio and have similar fabric.

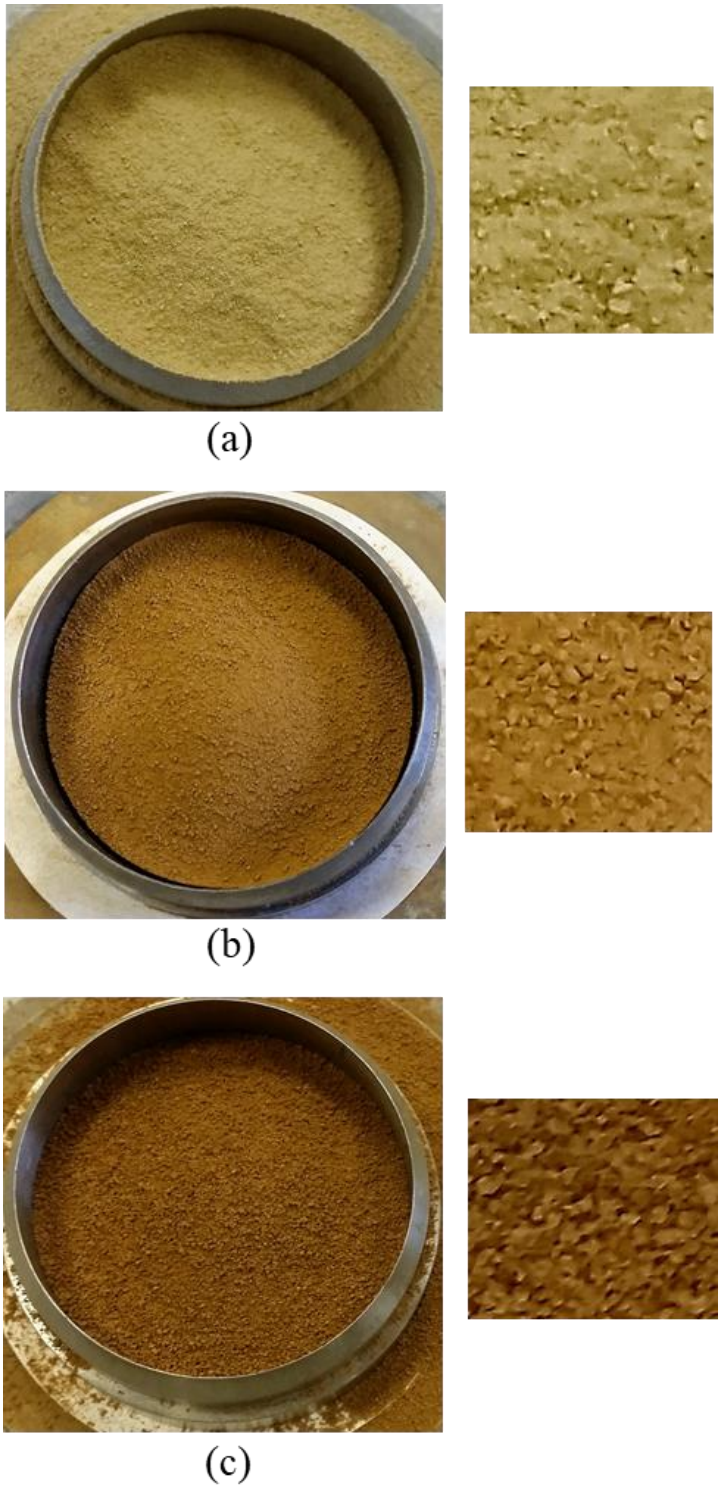

Figure 7. Samples post-freefall (overall oedometer ring and close-up image): (a) w_n = 0%; (b) w_n = 9%; (c) w_n = 15%. (N.B. oedometer ring of 50mm diameter)

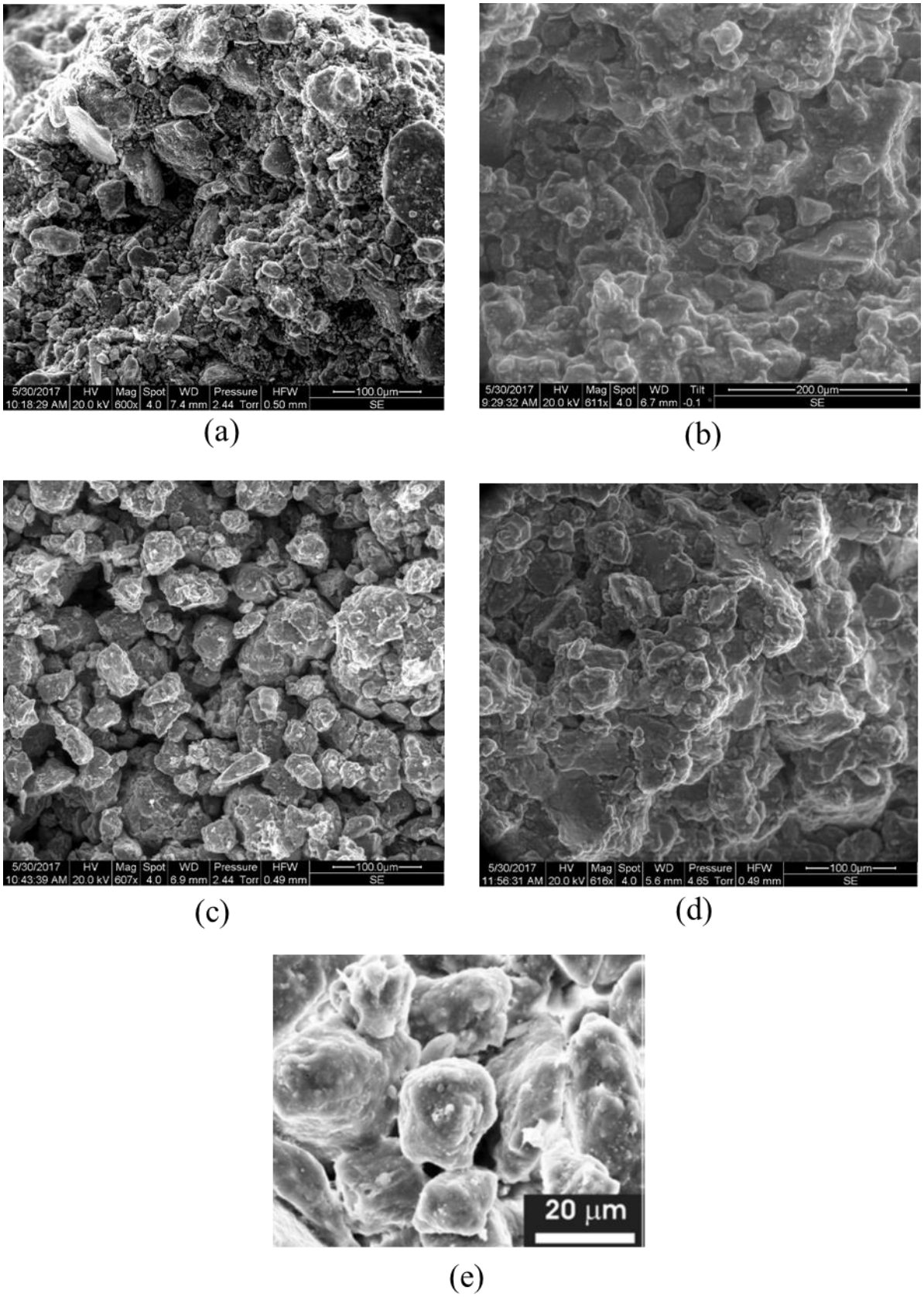

Figure 8. ESEM images of samples compressed to σ_v = 1600 kPa: (a) w_n = 0% pre-flooding; (b) w_n = 0% post-flooding; (c) w_n = 12% pre-flooding; (d) w_n = 12% post-flooding; (e) Image of intact loess taken from Milodowski et al. (2015).

Acknowledgements

The Authors thank Graham Keefe and Steve Ackerley in the geotechnical laboratory at Imperial College for their assistance in developing the freefall methodology and Peter Chung at the University of Glasgow's Imaging Spectroscopy and Analysis Centre (ISAAC) for his help with the ESEM imaging. The second author was funded by an EPSRC Doctoral Prize.

Data Statement

All data created during this research are openly available from http://dx.doi.org/10.5525/gla.researchdata.578

References

Assallay, A.M. 1998. Structure and hydrocollapse behaviour of loess. © Albashir Mohammed Assallay. Available from https://dspace.lboro.ac.uk/dspace-jspui/handle/2134/11230 [accessed 7 November 2017].

ASTM International. 2003. ASTM D5333-03: Standard Test Method for Measurement of Collapse Potential of Soils (Withdrawn 2012). ASTM International, West Conshohocken, PA.

ASTM International. 2014. ASTM D4546 - 14: Standard Test Methods for One-Dimensional Swell or Collapse of Soils. West Conshohocken, PA.

Barden, L., McGown, A., and Collins, K. 1973. The collapse mechanism in partly saturated soil. Engineering Geology, **7**(1): 49–60. Elsevier. doi:10.1016/0013-7952(73)90006-9.

BGS. 2016. BGS Lexicon of named rock units- Langley Silt Member. Available from http://www.bgs.ac.uk/lexicon/lexicon.cfm?pub=LASI [accessed 8 May 2019].

British Standards Institution. 1990. Methods of test for soils for civil engineering purposes. BS1377(2): Classification tests. British Standard Institution, Milton keynes, Uk,.

Feda, J. 1988. Collapse of loess upon wetting. Engineering Geology,. doi:10.1016/0013-7952(88)90031-2.

Head, K.H., and Epps, R.J. 2011. Manual of soil laboratory testing, permeability, shear strength and compressibility tests, Vol. 2. *In* 3rd edition. Whittles Publishing, Caithness.

Iriondo, M.H., and Kröhling, D.M. 2007. Non-classical types of loess. Sedimentary Geology, **202**(3): 352–368. Elsevier. doi:10.1016/j.sedgeo.2007.03.012.

Jefferson, I., and Ahmad, M. 2007. Formation of Artificial Collapsible Loess. *In* Problematic Soils and Rocks and In Situ Characterization. American Society of Civil Engineers, Reston, VA. pp. 1–10. doi:10.1061/40906(225)5.

Jennings, J.E., and Knight, K. 1975. A guide to construction on or with materials exhibiting additional settlement due to 'collapse' of grain structure. *In* Proceedings of the 6th African Conference on Soil Mechanics and Foundation Engineering. Durban. pp. 99–105.

Jiang, M., Hu, H., and Liu, F. 2012. Summary of collapsible behaviour of artificially structured loess in oedometer and triaxial wetting tests. Canadian Geotechnical Journal, **49**(10): 1147–1157. NRC Research Press. doi:10.1139/t2012-075.

Li, P., Vanapalli, S., and Li, T. 2016. Review of collapse triggering mechanism of collapsible soils due to wetting. Journal of Rock Mechanics and Geotechnical Engineering, **8**(2): 256–274. Elsevier. doi:10.1016/j.jrmge.2015.12.002.

Milodowski, A.E., Northmore, K.J., Kemp, S.J., Entwisle, D.C., Gunn, D.A., Jackson, P.D., Boardman, D.I., Zoumpakis, A., Rogers, C.D.F., Dixon, N., Jefferson, I., Smalley, I.J., and Clarke, M. 2015. The mineralogy and fabric of 'Brickearths' in Kent, UK and their relationship to engineering behaviour. Bulletin of Engineering Geology and the Environment, **74**(4): 1187–1211. Springer Berlin Heidelberg. doi:10.1007/s10064-014-0694-5.

Muñoz-Castelblanco, J. a, Pereira, J.M., Delage, P., and Cui, Y.J. 2011. Some aspects of the compression and collapse behaviour of an unsaturated natural loess. Géotechnique Letters, **1**(April-June): 17–22. Thomas Telford Ltd. doi:10.1680/geolett.11.00003.

Northmore, K.J., Bell, F.G., and Culshaw, M.G. 1996. The engineering properties and behaviour of the brickearth of south Essex. Quarterly Journal of Engineering Geology and Hydrogeology ,. doi:10.1144/GSL.QJEGH.1996.029.P2.04.

Pye, K. 1995. The nature, origin and accumulation of loess. Quaternary Science Reviews, **14**(7–8): 653–667. Pergamon. doi:10.1016/0277-3791(95)00047-X.

Rose, J., Lee, J.A., Kemp, R.A., and Harding, P.A. 2000. Palaeoclimate, sedimentation and soil development during the Last Glacial Stage (Devensian), Heathrow Airport, London, UK. Quaternary Science Reviews,. doi:10.1016/S0277-3791(99)00094-3.

Sides, G., and Barden, L. 1971. The Microstructure of Dispersed and Flocculated Samples of Kaolinite, Illite, and Montmorillonite. Canadian Geotechnical Journal, **8**(3): 391–399. NRC Research Press Ottawa, Canada . doi:10.1139/t71-041.

Smalley, I.J., and Marković, S.B. 2014. Loessification and hydroconsolidation: There is a connection. Catena,. doi:10.1016/j.catena.2013.07.006.

Wong, L.X. 2017. Experimental Evaluation of the Collapsibility of Unsaturated Brickearth. Imperial College London.

Zourmpakis, A., Boardman, D.I., and Rogers, C.D.F. 2005. Creation of artificial loess soils. *In* Unsaturated Soils: Experimental Studies. Springer-Verlag, Berlin/Heidelberg. pp. 123–134. doi:10.1007/3-540-26736-0_10.